Supporting Information

Adsorption mechanism and uptake of methane in Covalent Organic Frameworks: Theory and Experiment

José L. Mendoza-Cortés[1], Sang Soo Han[1,3], Hiroyasu Furukawa[2], Omar M. Yaghi*[,2] and William A. Goddard III*[,1]

[1]Materials and Process Simulation Center, California Institute of Technology, Pasadena, California 91125, USA, [2]Center for Reticular Chemistry, Department of Chemistry and Biochemistry, University of California-Los Angeles, 607 East Charles E. Young Drive, Los Angeles, California 90095, USA.

Present address: [3]Korea Research Institute of Standards and Science, Daejeon, 305-340, Republic of Korea.

E-mail: yaghi@chem.ucla.edu wag@wag.caltech.edu

Contents

List of Figures

1 Experimental methodology

Analytical techniques

Low pressure gas adsorption isotherms were measured volumetrically on an Autosorb-1 analyzer (Quantachrome Instruments). The CH_4 gas used was Ultra-high purity grade. For measurement of the apparent surface areas, the BET method was applied using the adsorption branches of the Ar isotherms assuming an Ar cross-sectional area of 14.2 $Å^2$/molecule. The micropore volumes (V_p) were determined using the Dubinin-Raduskavich (DR) transformed Ar isotherms across the linear region of the low pressure data. Elemental microanalyses, Thermal Gravimetric Analysis and Fourier transform infrared (FT-IR) spectra were obtained.

Synthesis of COF-5 and COF-8

All reactions were performed under nitrogen using either glove box or Schlenk line techniques. Anhydrous 1,4-dioxane (99.8%) and Acetone (99.8%, extra dry) was purchased from Acros Chemicals. Mesitylene (98%) was purchased from Fluka. 2,3,6,7,10,11-hexahydroxytriphenylene (HHTP) was purchased from TCI. 1,4-benzene diboronic acid (BDBA) was obtained from Aldrich Chemical Co. and 1,3,5-tris[(4-phenylboronic acid]benzene (BTPB) was prepared according to published procedures [1]. The experimental procedure it is the same as the literature [2], but the typical synthetic procedure for the synthesis of COF-8: A 60 mL vial was charged with BTPB (0.50 g, 1.14 mmol), HHTP (0.37 g, 1.14 mmol), and 50 mL of a 1:1v:v solution of mesitylene:dioxane. The resulting suspension was sonicated for 30 minutes at room temperature then placed at 85 °C for 3 days to afford a gray powder. The resulting powder was filtered off and was washed with dry acetone (3x20 mL). Then it was activated with acetone (2x50 mL) for 2 days then dried at 85 85 °C/10^{-5} torr to afford COF-8 as gray powder (0.53 g, 71%). Anal. Calcd. for C14H7BO2: C, 77.13; H, 3.24. Found: C, 76.39; H, 4.19.

Gravimetric high-pressure gas adsorption measurements for COF-5 and COF-8

Gravimetric CH_4 sorption isotherms were measured by use of a GHP-300 (Gravimetric High Pressure analyzer) from the VTI Corporation [3]. A Rubotherm magnetic suspension balance MC-5 was used to measure the change in mass of samples suspended within a tube (22 mm i.d.) constructed from Inconel 625 under a chosen atmosphere. Prior to admittance of the analyte gas, the entire chamber and manifold were evacuated at room temperature, and the weight of the Al sample bucket (12 mm i.d. 6 21 mm length) was measured. After loading the COF-5 (or COF-8) sample

(ca. 200 mg) the system was purged at room temperature with CH_4 and helium, and the sample was outgassed, using a turbomolecular drag pump (Pfeiffer, TSH 071 E), until a constant mass was attained. When CH_4 gas was used, water and other condensable impurities were removed with a LN_2 trap. Pressure was measured with a MKS Baratron transducer 120AA (0 to 1000 Torr) and an electronic Bourdon gauge-type transducer (Mensor, up to 1500 psi). The adsorbate was added incrementally, and data points were recorded when no further change in mass was observed. The temperature in the Inconel tube was also monitored with a platinum resistance thermometer. To obtain the excess adsorption isotherm, all data points were corrected for buoyancy and the thermal gradient that arises between the balance (313 K) and the sample bucket (298 K). Buoyancy and thermal-gradient effects exhibited by the bucket and the components associated with the magnetic suspension balance were corrected on the basis of the change in mass of the empty bucket within the analyte gas at 298 K. The weight loss due to the buoyancy of the adsorbent was determined by multiplying the volume of the COF-5 (or COF-8) framework skeleton by the density of CH_4 [4] (i.e., corrected mass for buoyancy is $V_{\text{skeleton}} \times \rho_{\text{bulk}}$). The volume of the COF-5(or COF-8) framework skeleton was determined from the helium (<15 bar) buoyancy curve at 298 K using the same gravimetric system [5]. The absolute amount of gas adsorbed was calculated from the density of the framework skeleton (inverse of the skeleton volume) and the crystallographic density, leading to an accessible pore volume (V_{p}).

The results of pore volume at high pressure from He at high pressure (Up to 80 bar) were compared to those obtained from low pressure (1 bar) Argon isotherms (Figure S1). This match confirms the good quality of the sample, however we are considering ideal samples without any external surface but only an internal pore system, while real crystalline samples: (1)have finite size (i.e., sub-millimeter scale), (2)may be partly decomposed, (3)might contain small amount of guest molecules [6]. Considering that estimation of the true density of porous materials is not easy [5], it is difficult to conclude which value reflects an actual system. However, we cannot fully exclude the possibility of helium adsorption on the COF-5 (or COF-8) surface. Therefore these V_{p} values does not match completely to those estimated from theory where we have considered fully ideal compounds. On the other hand the matching in the sorption isotherms is fairly good, this might suggest that the models in theory and experiment of the estimation of V_{p} are not self-consistent but the models for sorption are.

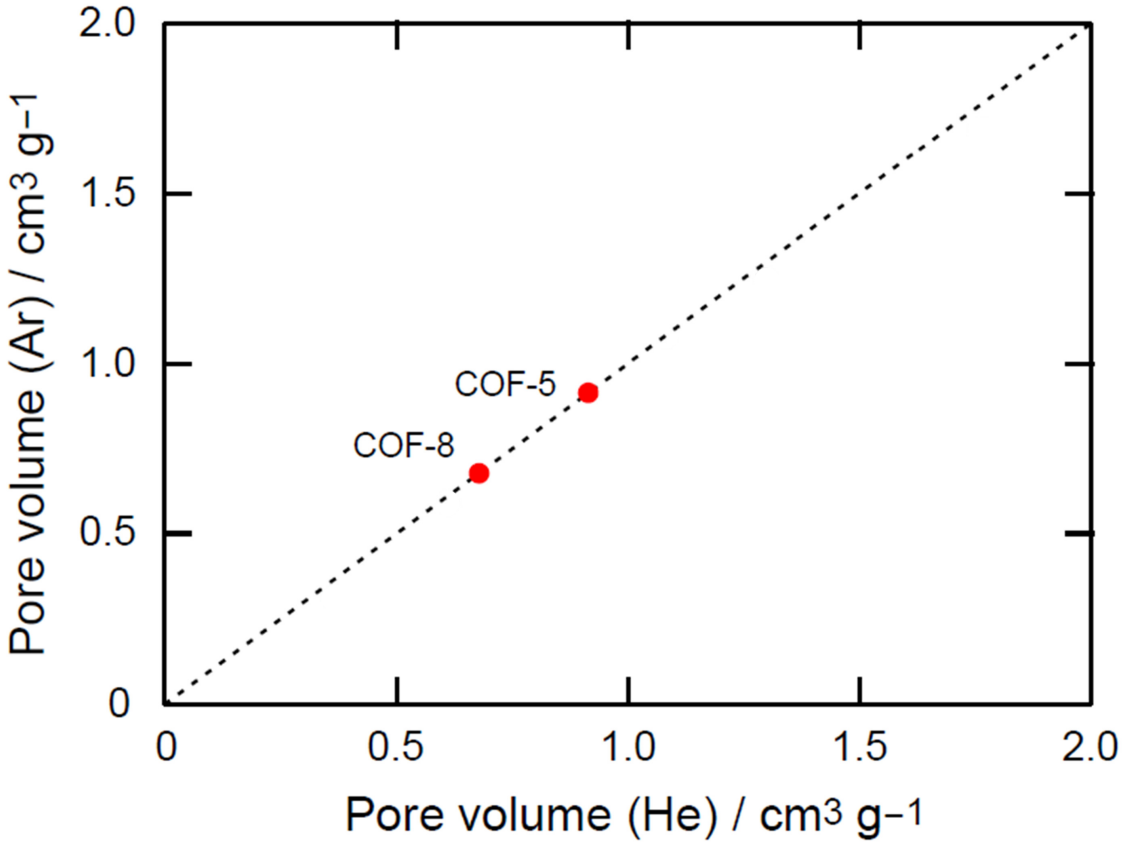

Figure S1: Comparision of pore volume at different pressures of COF-5 and COF-8

2 Grand Canonical Monte Carlo

In the Grand Canonical ensemble the independent variables are: chemical potential (μ), volume (V) and temperature (T). Here the volume belongs to the cavity of the porous material. First some molecules are placed in the cavity fo the structure, each atoms has a position vector associate with it in a coordinate system. Four events are taking into account in the simulation: translation, rotation, creation and anhilation. The code implemented is based in a standard algorithm [14][15].

In a translation event, the new components of the position vector, $\mathbf{R}$ are given by:

$$\begin{aligned} R_x^{new} &= R_x^{old} + \delta u \\ R_y^{new} &= R_y^{old} + \delta v \\ R_z^{new} &= R_z^{old} + \delta w \end{aligned}$$

where u, v and w are random numbers localized between - 1 and 1, and δ is a constant.

The new orientation vector (event), $\mathbf{O}$, is determined by:

$$\begin{aligned} O_x^{new} &= \frac{l}{2}\frac{u}{r} \\ O_y^{new} &= \frac{l}{2}\frac{v}{r} \\ O_z^{new} &= \frac{l}{2}\frac{w}{r} \end{aligned}$$

and,

$$r = \sqrt{u^2 + v^2 + w^2}$$

Where u, v and w are random numbers localized between - 1 and 1, and l is the bondlength. A decision is taken in order to accept or refuse the new configuration based on the probability, P_{move}

$$P_{move} = min[\exp(-\Delta U/kT); 1] \tag{1}$$

where

$$\Delta U = U_{new} - U_{old} \tag{2}$$

The second part of the simulation process of the GCMC is to add or remove a molecule [14][15]. These two events are generated at random with equal probability.

If the event addition is generated then the next step is the random generation of the position and the orientation of new molecule(s). The potential of this new configuration is calculated and it is accepted or refejected based on, P_{add}:

$$P_{add} = min\left[\frac{1}{N+1}\frac{PV}{kT}\exp(-\Delta U/kT); 1\right] \tag{3}$$

Here N is the number of molecules before the addition event is taken place, P is the pressure of the bulk gas, and V is the volume of the porous material cavity.

If the event annihilation is generated then the next step is deletion of a randomly chosen molecule of the gas phase. Once again the potential of the new configuration is calculated, and the event is accepted or rejected based on P_{anh}:

$$P_{anh} = min\left[\frac{NkT}{PV}\exp(-\Delta U/kT); 1\right] \tag{4}$$

Where N is the number of molecules before the subtraction. If the annihilation event is accepted, then the substraction is made permanent. If the subtraction is rejected, then the deleted molecule is returned to its old position.

3 Basis Set Superposition Error calculations

For every interaction, four clusters were considered, where the resolution of the identity (**RI**) second order Møller–Plesset perturbation theory (RI-MP2) calculations (**RI-MP2**) [12][13] were implemented in the TURBOMOLE program [11][10].

The Basis Set Superposition Error ($BSSE$) was corrected using the Countepoise Method CP [7] for each of model. The CP method calculates each of the units with the basis functions of the other (but without the nuclei or electrons), using the so called *ghost orbitals* [8]

CH_4–CH_4 interaction

In order to calculate the properties of the intereactions in CH_4–CH_4, four symmetries were studied: *C_{3v}-1*, *C_{3v}-2*, *D_{3d}* and *D_{3h}*. For each structure the theoretical methodology was applied and the data is plotted for each configuration in the Figure S2.

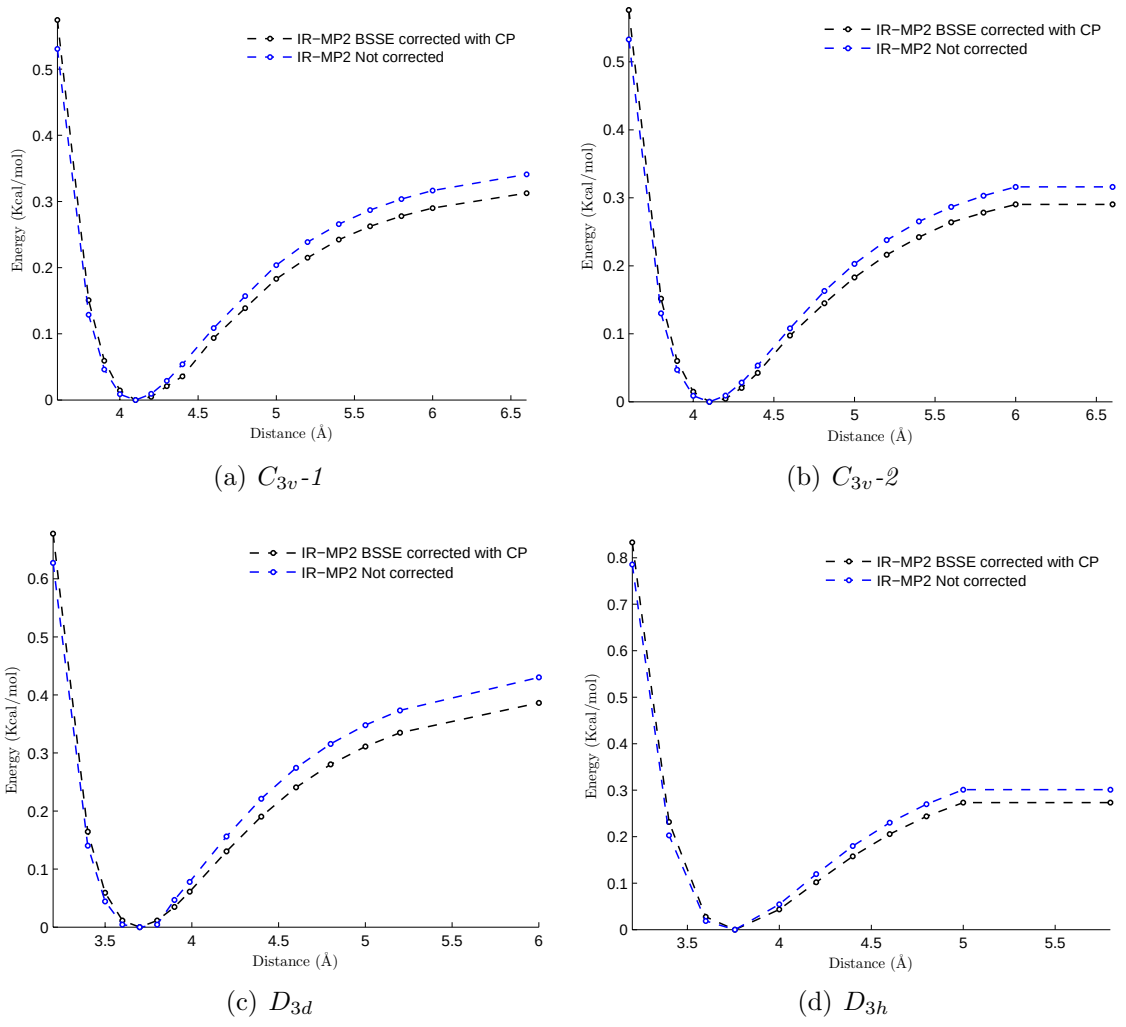

(a) *C_{3v}-1* (b) *C_{3v}-2*

(c) *D_{3d}* (d) *D_{3h}*

Figure S2: BSSE correction for each cluster of the CH_4–CH_4 interaction

C_6H_6–CH_4 interaction

In order to calculate the properties of the intereactions in C_6H_6–CH_4 four symmetries were studied: ANTI (C_{3v}-*1*), SYN (C_{3v}-*2*), ANTI2 (C_{3v}-*3*) and SYN2 (C_{3v}-*4*). For each structure the **IR-MP2** calculation method was applied, then the BSSE was applied using the *CP* method. The data is plotted for each configuration in the Figure S3.

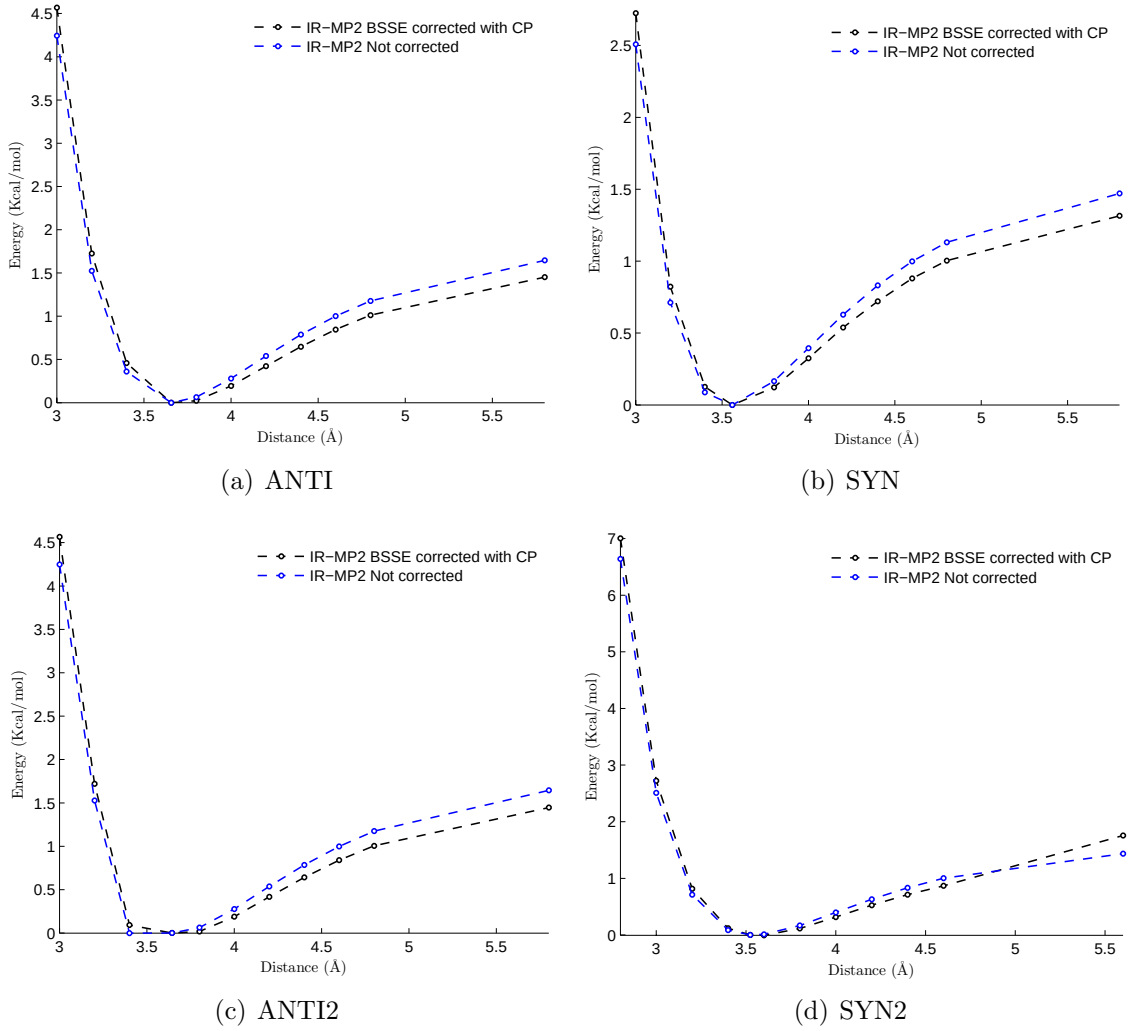

(a) ANTI (b) SYN

(c) ANTI2 (d) SYN2

Figure S3: BSSE correction for each cluster of the C_6H_6–CH_4 interaction

$B_3O_3H_3$–CH_4 interaction

In order to calculate the properties of the intereactions in $B_3O_3H_3$–CH_4 four symmetries were studied: ANTI (C_{3v}-*1*), SYN (C_{3v}-*2*), ANTI2 (C_{3v}-*3*) and SYN2 (C_{3v}-*4*). For each structure the **IR-MP2** calculation method was applied, then the BSSE was applied using the *C*P method. The data is plotted for each configuration in the Figure S4.

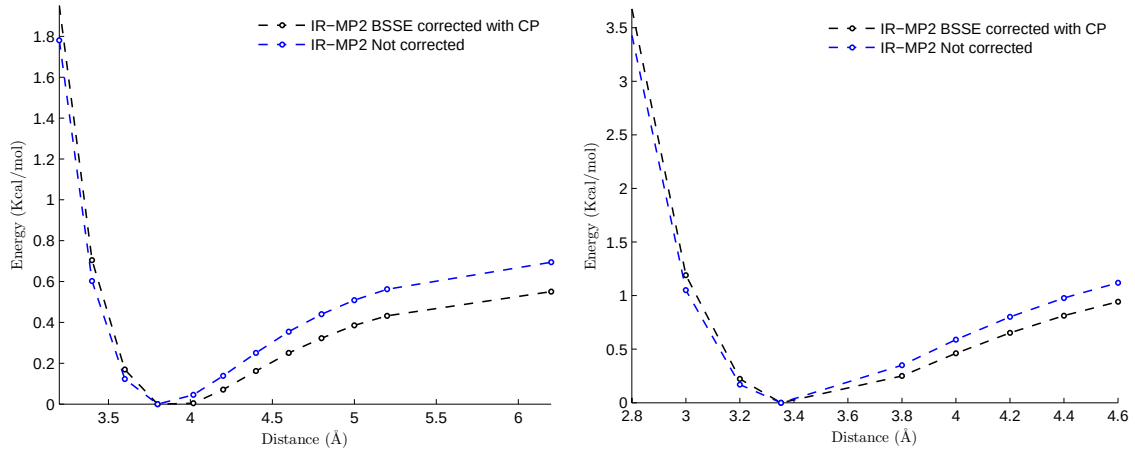

(a) ANTI (b) SYN

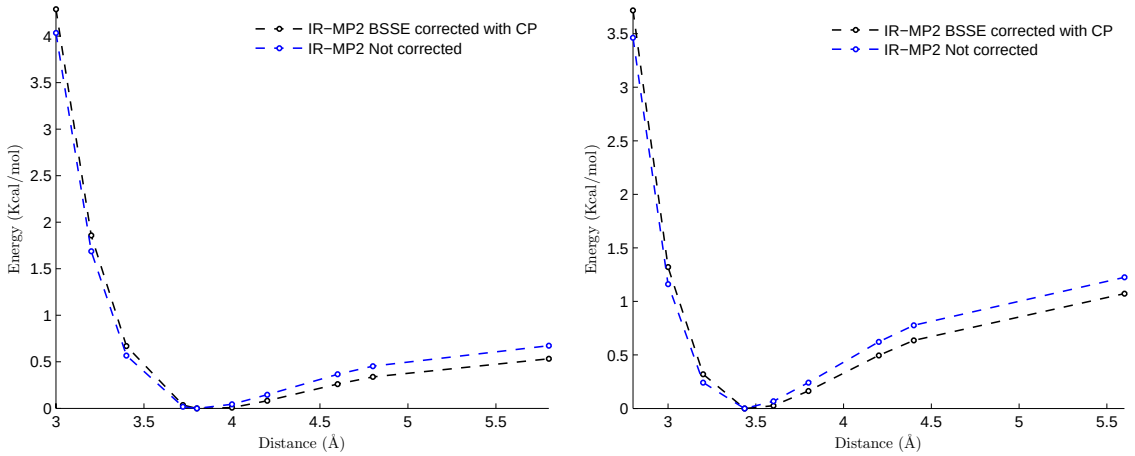

(c) ANTI2 (d) SYN2

Figure S4: BSSE correction for each cluster of the $B_3O_3H_3$–CH_4 interaction

$Si(CH_4)_4$–CH_4 interaction

In order to calculate the properties of the intereactions in $Si(CH_4)_4$–CH_4 four symmetries were studied: ANTI C_{3v}-*1*, SYN C_{3v}-*2*, ANTI2 C_{3v}-*3* and SYN2 C_{3v}-*4*. was applied using the *C*P method. The data is plotted for each configuration in the Figure S5.

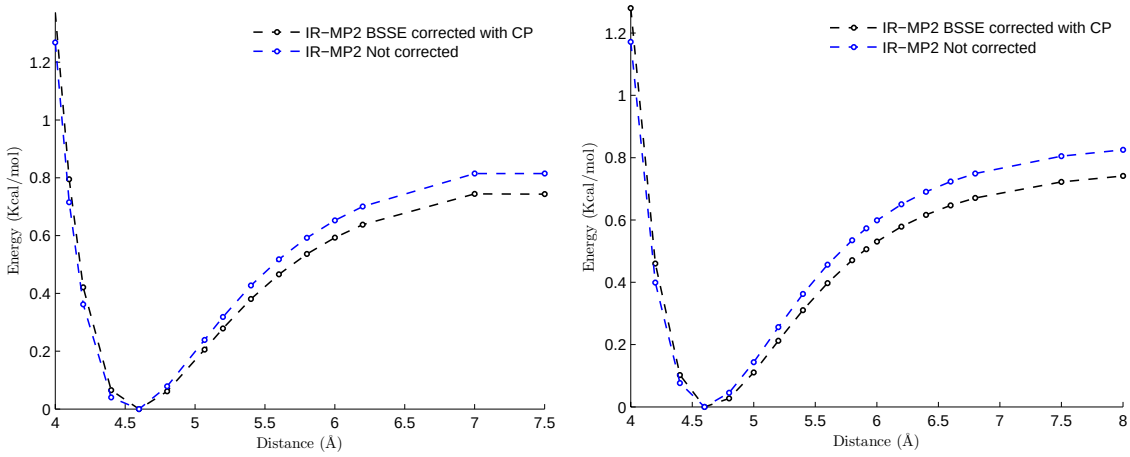

(a) ANTI

(b) SYN

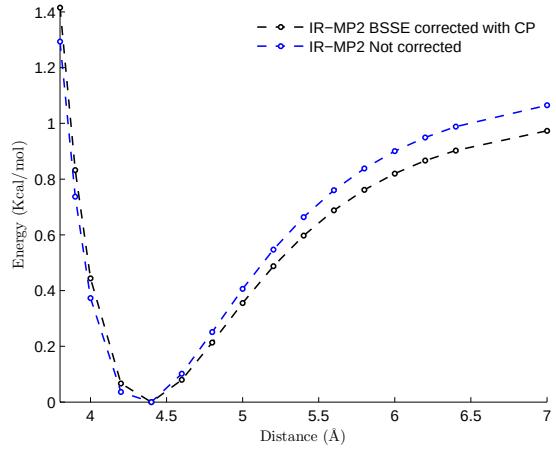

(c) ANTI2

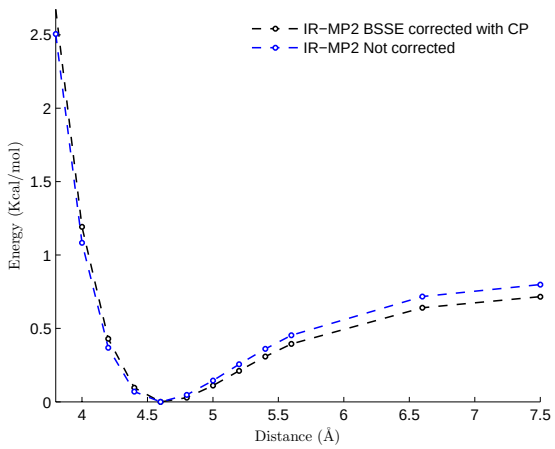

(d) SYN2

Figure S5: BSSE correction for each cluster of the $Si(CH_4)_4$–CH_4 interaction

4 Structures of the edge interaction

The structures used to find the interaction energy with the edge of the organic linker are shown in S6

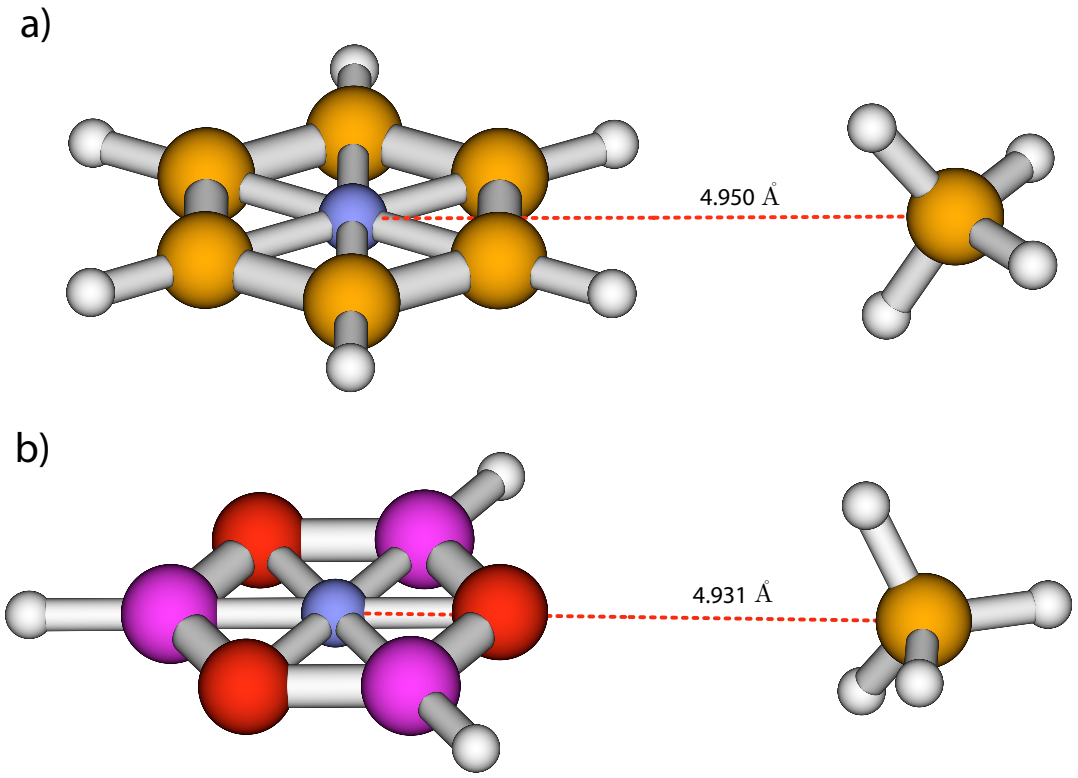

Figure S6: Equilibrium structure found to obtain the binding energy a) BEN-CH_4 and b)BOR-CH_4. C is orange, H is white, O is red, B is pink. The blue one is a dummy atom to show the barycenter of the molecule.

5 Equation of state for methane: experiment vs simulation

To further validate our GCMC methodology and our developed FF, we estimated the density of methane at different temperatures (260-400 K) and pressures (1, 10 and 100 bar). The results from theory were compared with those from experiments (Figure S7) [16]. Our simulations show a negative deviation at 100 bar. Since greater deviation was observed at low temperature (260 K), the difference may be attributed to condensation phenomena of methane in the real system, but we did not consider. On the other hand, estimated density at 1 and 10 bar was overestimated at whole temperature range we simulated, especially at high temperature region. One of the reasons may be overestimation of methane-methane interaction. However, the error near the ambient temperature is not significant; therefore, potential error in our simulations should not mislead to adsorption behaviors. More importantly, since the density at high pressure region is underestimation, estimated methane uptake should not be overestimated.

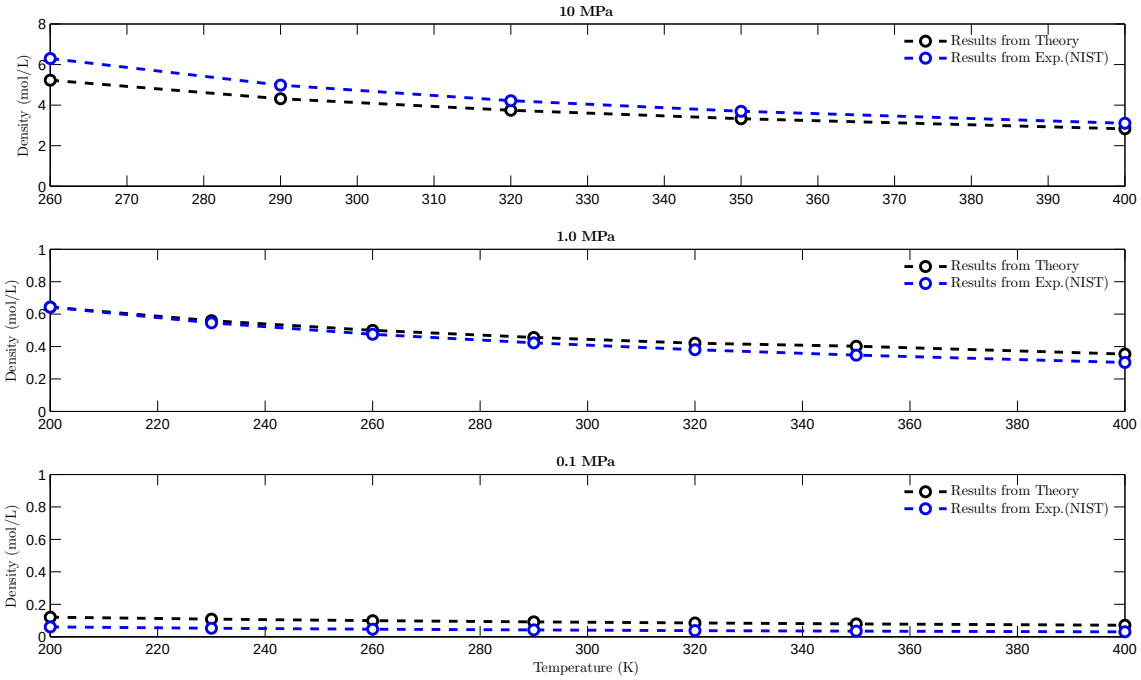

Figure S7: Methane density calculated from theory and experiment at different pressures (1, 10, 100 bar as a function of temperature (260-400 K).

6 Comparison between theoretical and experimental methane adsorption isotherms of MOF-177

Using the mixing rules with our current parameters for the organic linkers and methane and out previous [17] parameters for MOF-177, we calculated the CH_4 uptake. This was then compared to experimental data available (Figure S8). The experimental data has not been reported in the literature yet.

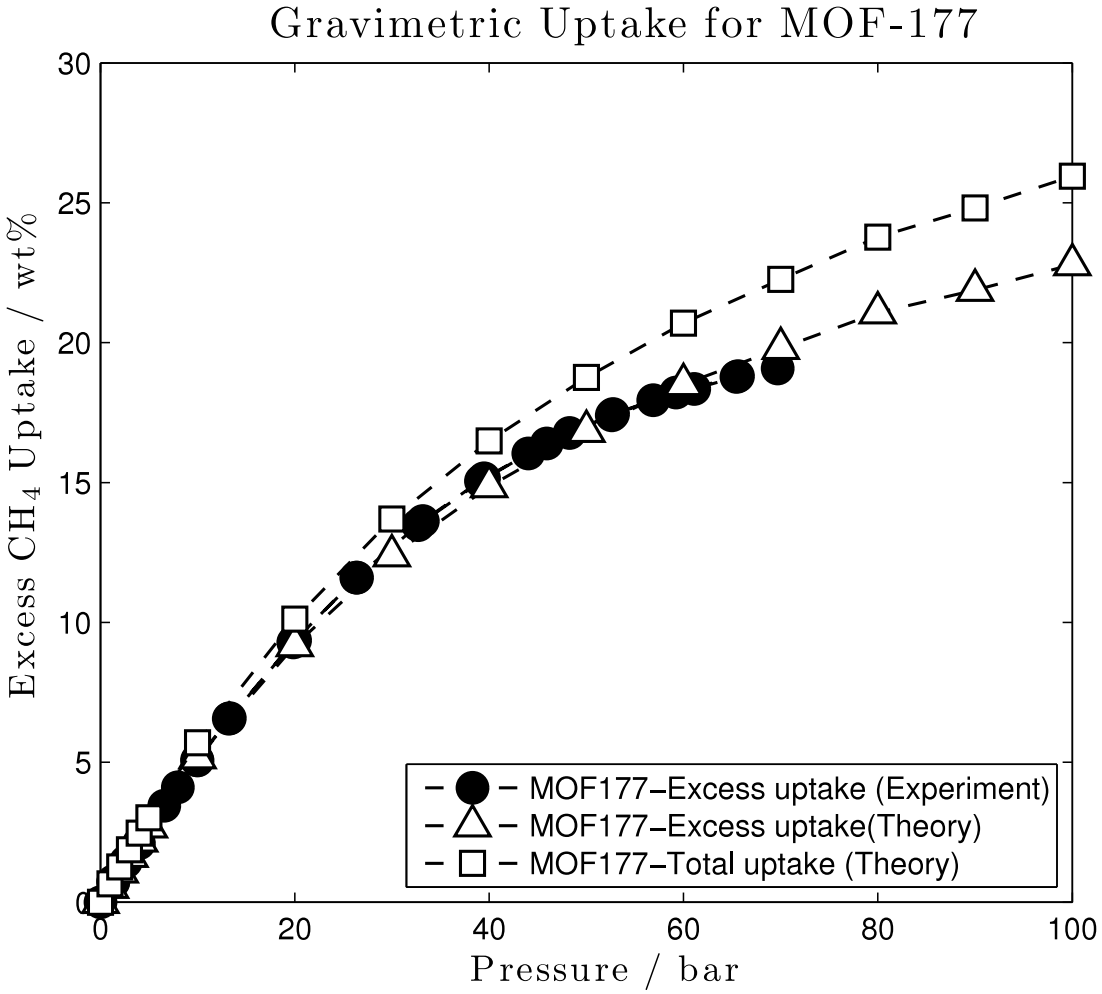

Figure S 8: Predicted (open triangles) and experimental (closed circles) methane isotherms at 298 K in excess uptake gravimetric units (wt%). Total predicted uptakes is shown in open squares.

7 GCMC snapshots taken for COF-1

In the main text we showed that the average of all the GCMC steps, however in this section we are showing only the snapshot at the end of the simulation for COF-1. The purpose of this section is to demonstrate that only three molecules of methane are able to enter in the pore of COF-1 even at 100 bar, this can be observed in Figure S9.

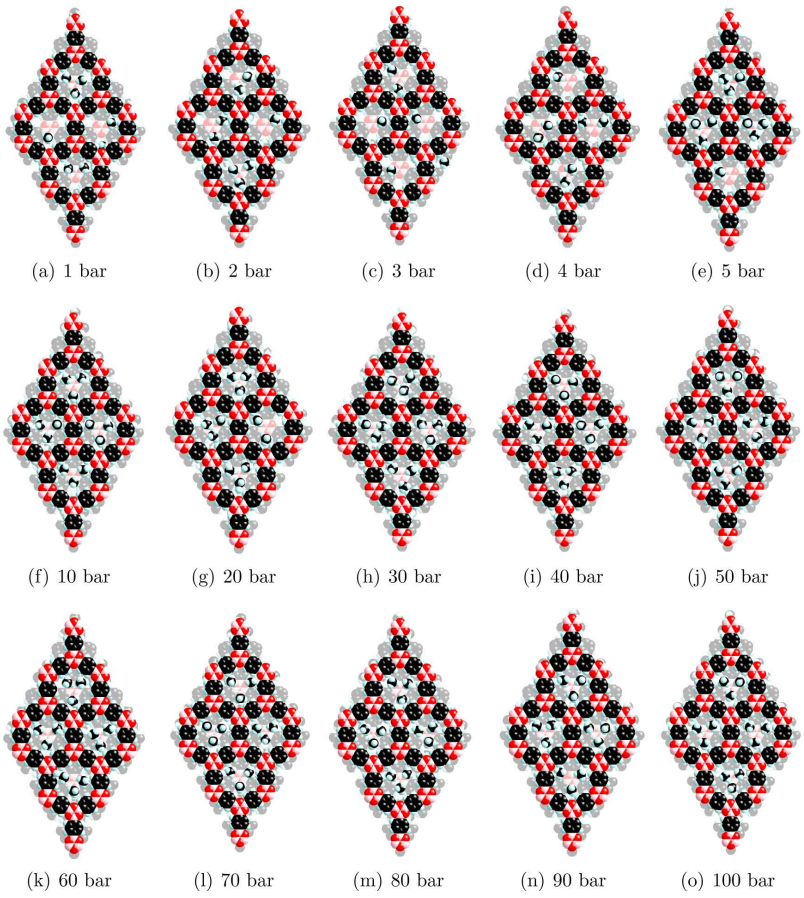

Figure S9: Snapshots taken of the supercell of COF-1 at the end of the simulation. The unit cell is not shown. Atoms colors: B:pink, O:red, C:black and H:blue.

8 Analysis of total vol. uptake from 1-100 bar

To the best of our knowledge, the dependence of the sorption is viewed as two variables at the time, i.e. uptake *vs* surface area (S_A), uptake *vs* density (ρ), uptake *vs* pore volume (Vp) and uptake *vs* Qst.

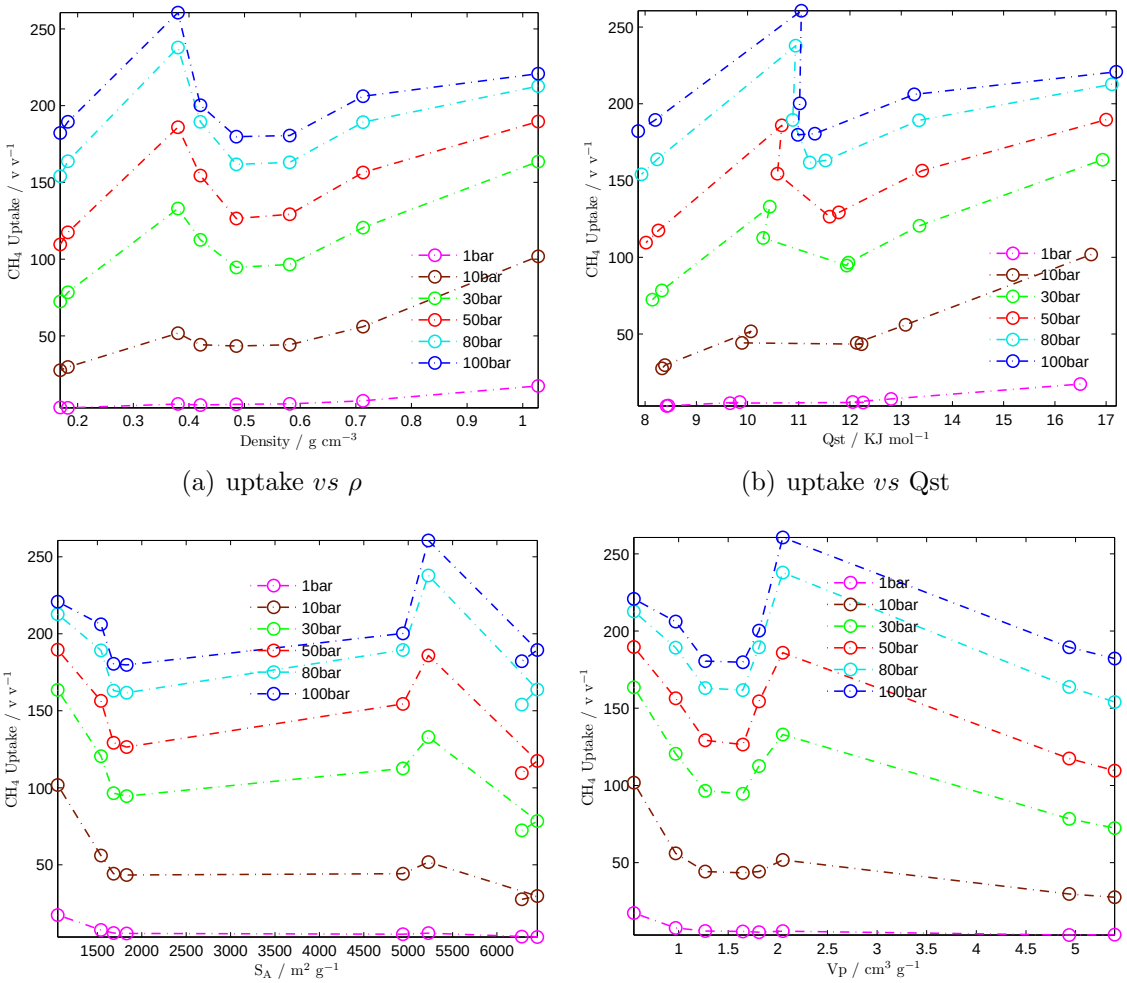

(a) uptake *vs* ρ

(b) uptake *vs* Qst

(c) uptake *vs* S_A

(d) uptake *vs* Vp

Figure S10: Relation of (Qst, ρ , S_A, Vp) *vs* Uptake. Dotted lines are used to help the eye

However these do not tell us about the interdepence of these variables. Therefore we decided to explore the dependence of two variables at the time with respect to the uptake on all the materials to see if there is a clear relation among them.

The Figure S11 show this analysis between these variables:

Uptake	*vs*	ρ	*vs*	Qst	Fig. S11(a)
Uptake	*vs*	ρ	*vs*	S_A	Fig. S11(b)
Uptake	*vs*	ρ	*vs*	Vp	Fig. S11(c)
Uptake	*vs*	Qst	*vs*	S_A	Fig. S11(d)
Uptake	*vs*	Qst	*vs*	Vp	Fig. S11(e)
Uptake	*vs*	Vp	*vs*	S_A	Fig. S11(f)

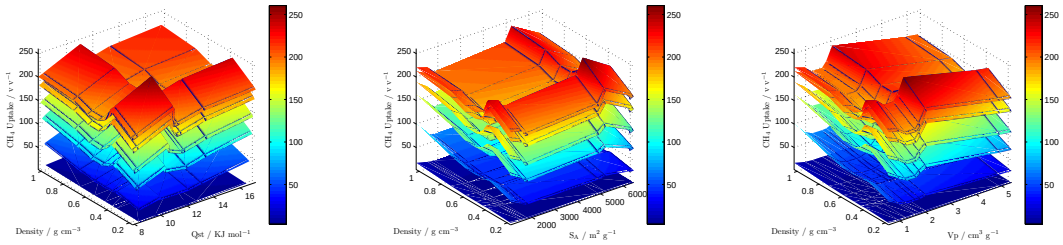

(a) uptake *vs* ρ *vs* Qst (b) uptake *vs* ρ *vs* S_A (c) uptake *vs* ρ *vs* Vp

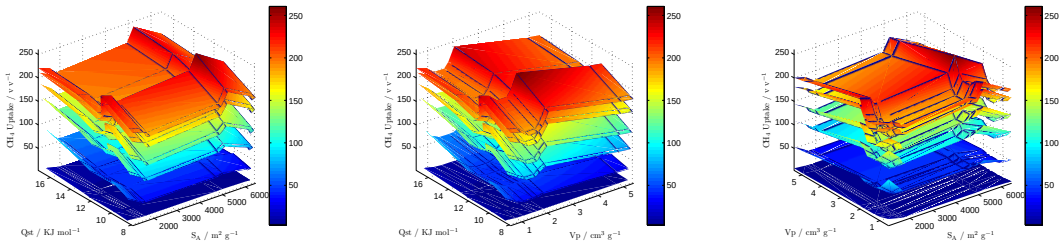

(d) uptake *vs* Qst *vs* S_A (e) uptake *vs* Qst *vs* Vp (f) uptake *vs* Vp *vs* S_A

Figure S11: Dependence of uptake with respect to ρ, Qst, PV and S_A in total volumetric uptake units. In each subgraph, six pressures are shown: 1(dark blue), 10(blue), 30(light blue), 50(green), 80(yellow) and 100(red) bar.

Uptake *vs* density *vs* Qst

In Figure S11(a), we analized the dependence: uptake *vs* density *vs* Qst. Then if we take every surface and make a contour plot we obtain Figure S13 which shows that there are three maxima at the pressure 30 bar, that in absolute uptake units corresponds to:

Qst / KJ mol^{-1}	Density / g cm^{-3}
16.95	0.38
16.95	1.03
11.05	0.38

However, in delivery amount units, there are four maxima at 30 bar which are (graph is not shown):

Qst / KJ mol^{-1}	Density / g cm^{-3}
16.95	0.38
16.95	1.03
10.66	1.03
11.05	0.38

Furthermore, in the case of methane uptake in COFs, the variable ρ is proportional to Qst (Figure S12).

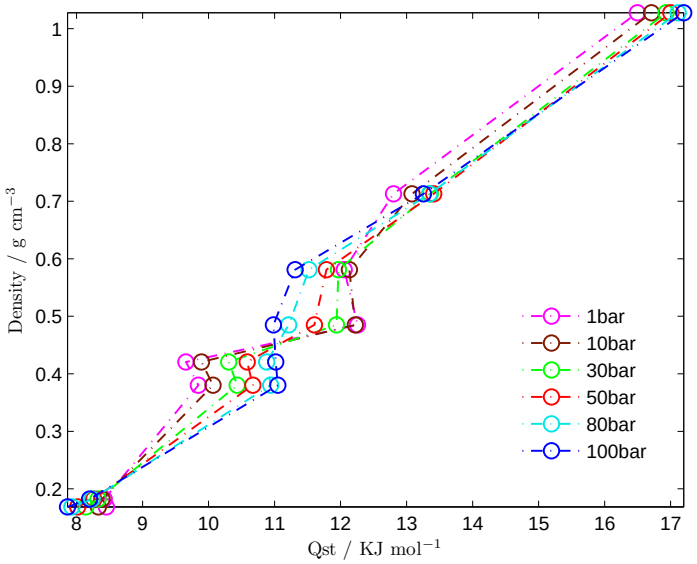

Figure S12: Relation of density *vs* Qst. The dotted lines are plotted in order to help the eye

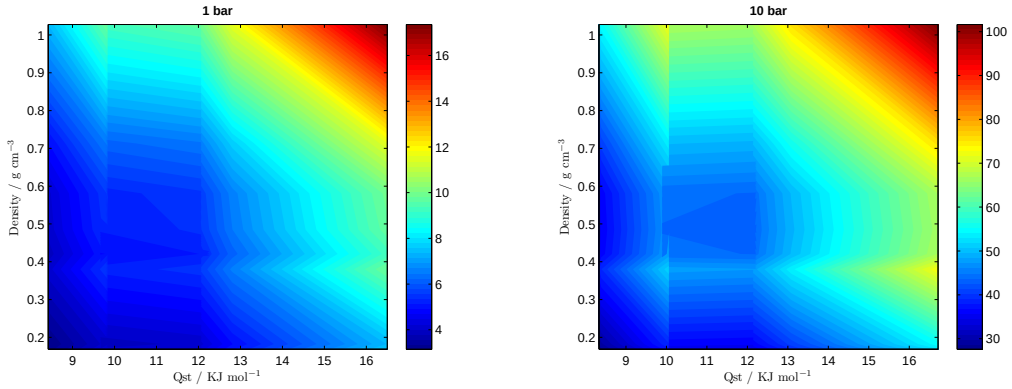

(a) 1 bar

(b) 10 bar

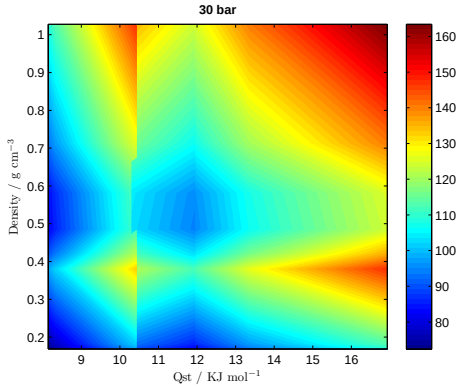

(c) 30 bar

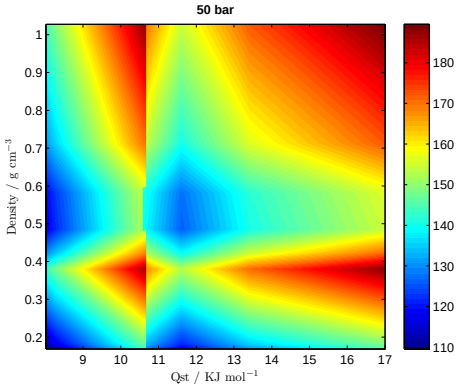

(d) 50 bar

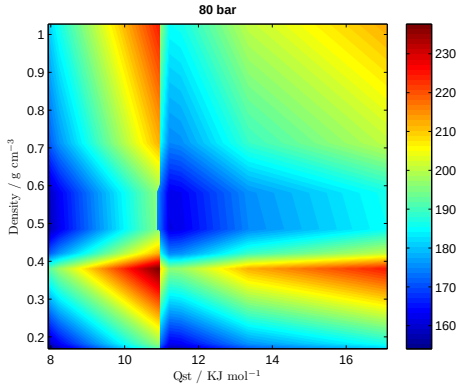

(e) 80 bar

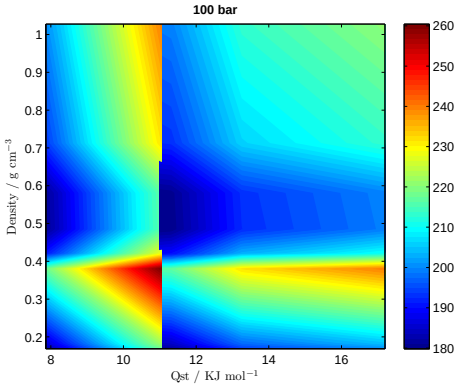

(f) 100 bar

Figure S13: Contour graph of density *vs* Qst. Three maxima can be found at 30 bar, while at 50 bar four maxima can be observed, these remains at 80 and 100 bar

Uptake *vs* density *vs* S_A

In Figure S11(b), we analized the dependence: uptake *vs* ρ *vs* S_A. Then if we take every surface and make a contour plot we obtain Figure S13 which shows that there are four maxima at the pressure 30 bar, that in absolute uptake units corresponds to:

Density / g cm^{-3}	S_A / m^2 g^{-1}
0.38	1050
1.03	1050
0.38	5230
1.03	5230

In delivery amount units, these are the same four maxima at 30 bar (Graph is not shown). Furthermore, in the case of methane uptake in COFs, it seems that ρ is inversely proportional to S_A (Figure S14). There two parts in the relation where 2D-COFs have a bigger slope (left in the graph) while 3D-COFs have a less dependent relation (on the right of the graph).

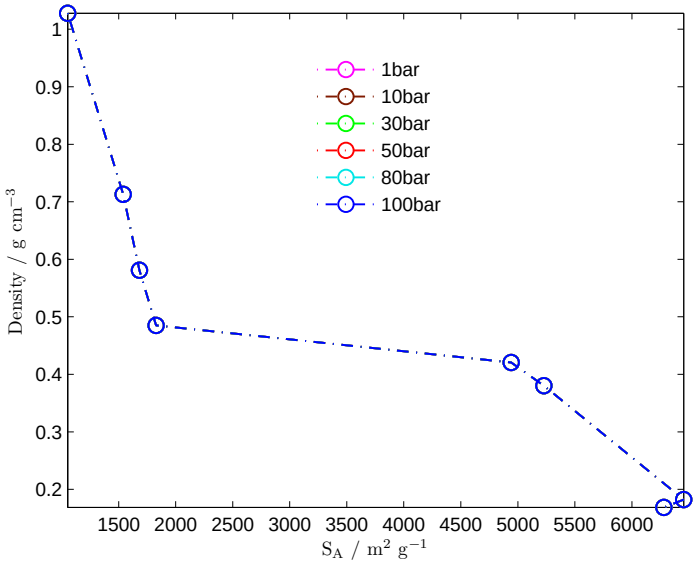

Figure S14: Relation of density *vs* S_A. The dotted lines are plotted in order to help the eye

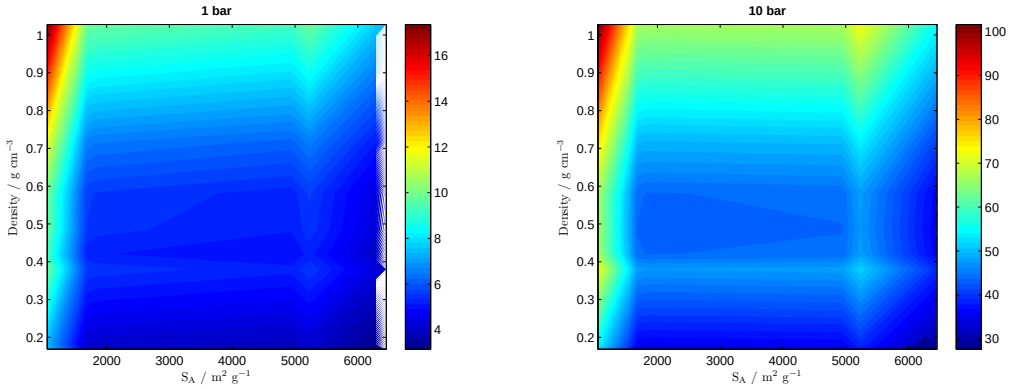

(a) 1 bar

(b) 10 bar

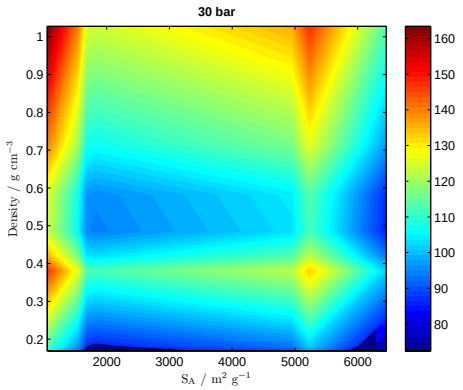

(c) 30 bar

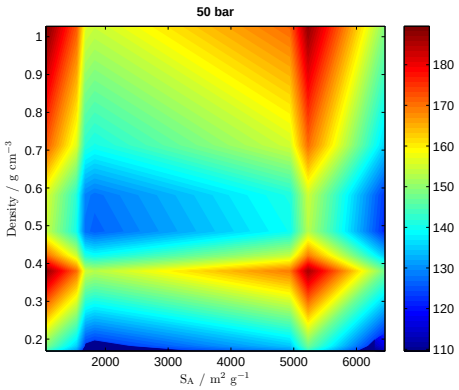

(d) 50 bar

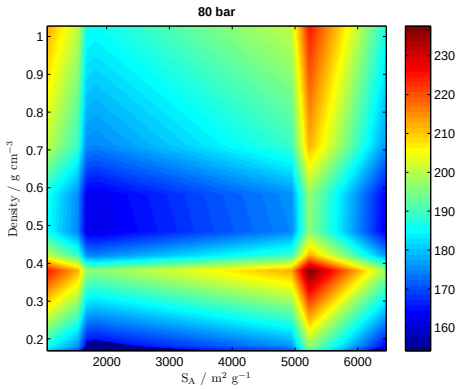

(e) 80 bar

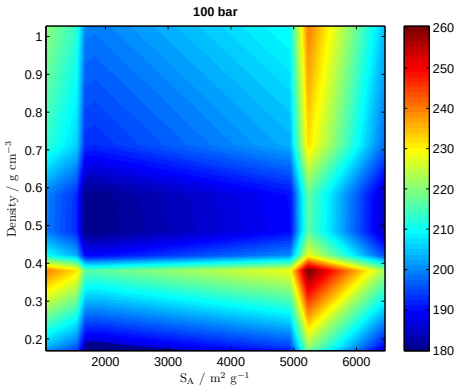

(f) 100 bar

Figure S15: Contour graph of density *vs* S_A. At 1 or 10 bar there are not clear maxima.

Uptake *vs* density *vs* Vp

In Figure S11(c), we analized the dependence: uptake *vs* ρ *vs* Vp. Then if we take every surface and make a contour plot we obtain Figure S13 which shows that there are three maxima at the pressure 30 bar, that in absolute uptake units corresponds to:

Density / g cm^{-3}	Vp / cm^3 g^{-1}
0.38	0.55
1.03	0.55
1.03	2.05

However, in delivery amount units, there are four maxima at 30 bar which are (graph is not shown):

Density / g cm^{-3}	Vp / cm^3 g^{-1}
0.38	0.55
1.03	0.55
1.03	2.05
0.38	2.05

Furthermore, in the case of methane uptake in COFs, it seems that ρ is inversely proportional to Vp (Figure S16), however, the two steps relation separating 2D-COFs from 3D-COFs is no longer observed. Of course there is not a theoretical reason for the dotted line to exist, except that to help the eye.

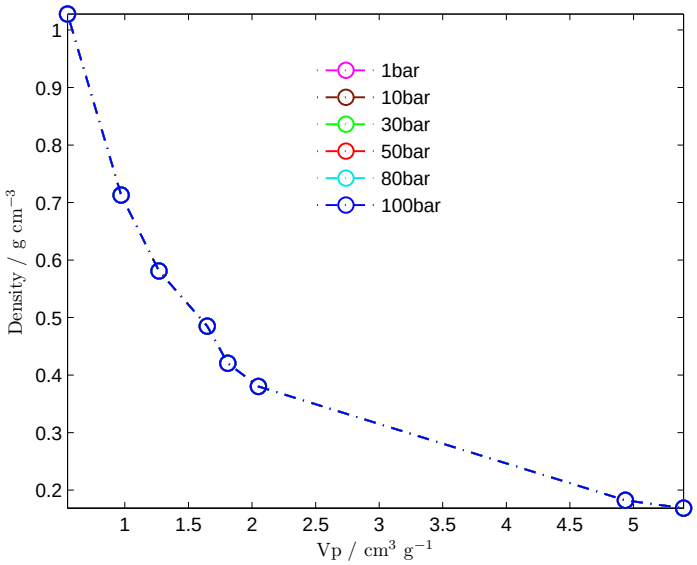

Figure S16: Relation of density *vs* Vp.

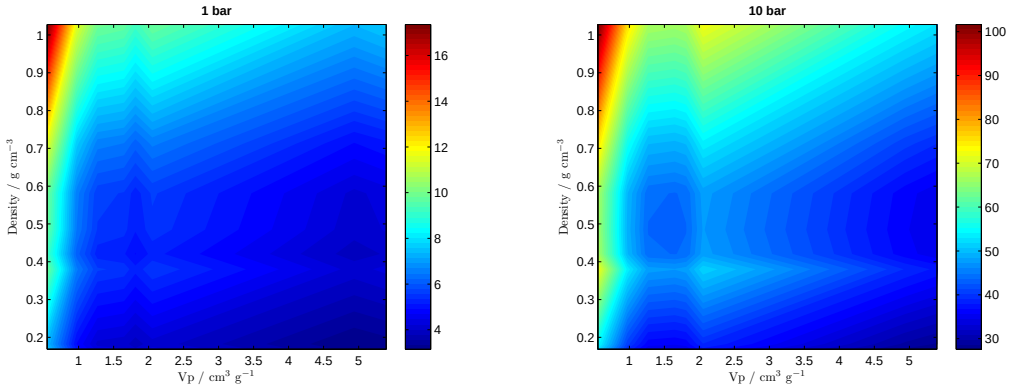

(a) 1 bar

(b) 10 bar

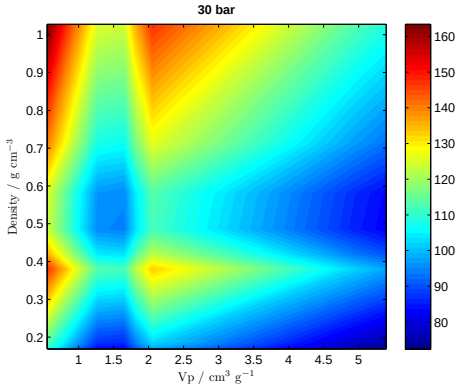

(c) 30 bar

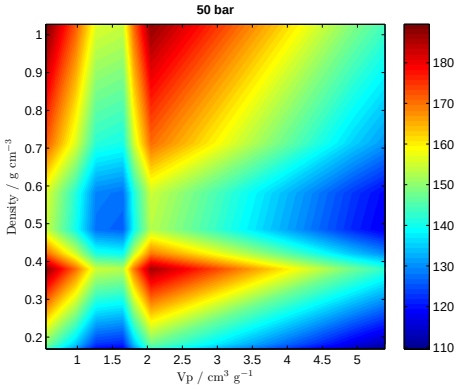

(d) 50 bar

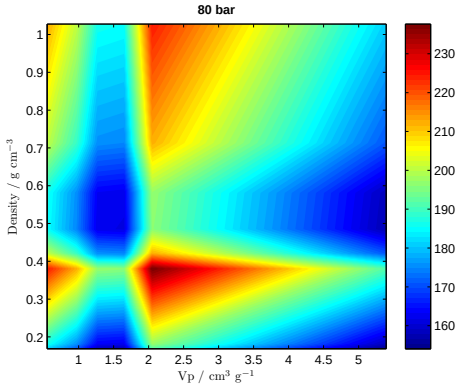

(e) 80 bar

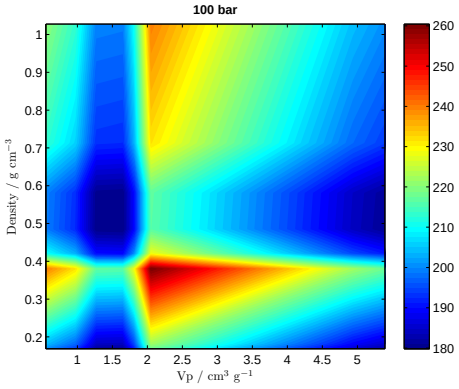

(f) 100 bar

Figure S17: Contour graph of density *vs* Vp. At 1 and 10 bar, maximum points are not clearly observed

Uptake *vs* **Qst** *vs* $\mathbf{S_A}$

In Figure S11(d), we analized the dependence: uptake *vs* Qst *vs* S_A. Then if we take every surface and make a contour plot we obtain Figure S19 which shows that there are three maxima at the pressure 30 bar, that in absolute uptake units corresponds to:

Qst / KJ mol^{-1}	S_A / m^2 g^{-1}
16.9	1050
10.4	1050
16.9	5230

However, in delivery amount units, there are four maxima at 30 bar which are (graph is not shown):

Qst / KJ mol^{-1}	S_A / m^2 g^{-1}
16.9	1050
10.9	1050
16.9	5200
10.4	5200

Furthermore, in the case of methane uptake in COFs, it seems that Qst is inversely proportional to S_A (Figure S18). There two steps in this relation where 2D-COFs have a larger slope (left in the graph) while 3D-COFs have a smaller one (on the right of the graph), this is a similar behaviour to the one of density *vs* S_A.

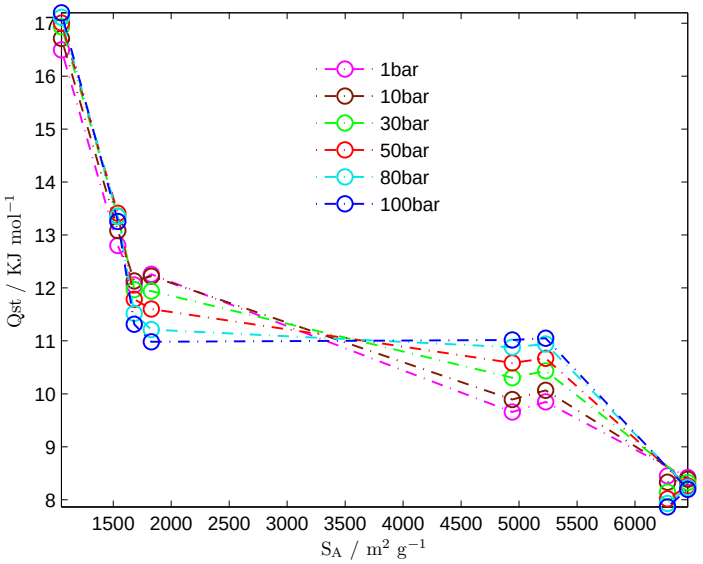

Figure S18: Qst *vs* S_A

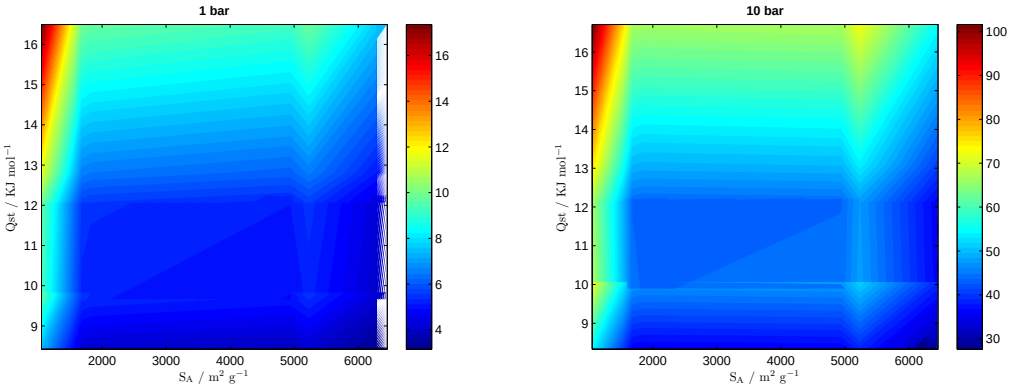

(a) 1 bar

(b) 10 bar

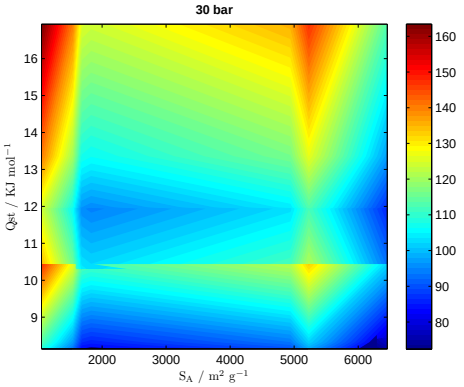

(c) 30 bar

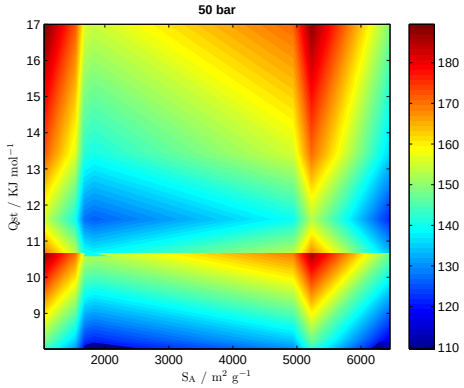

(d) 50 bar

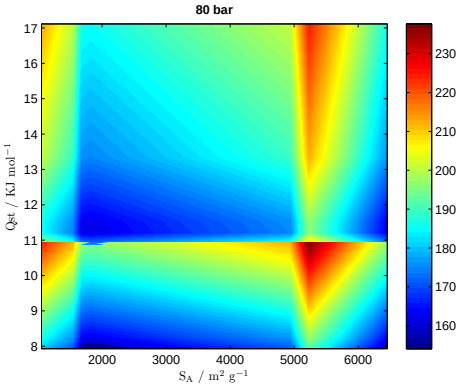

(e) 80 bar

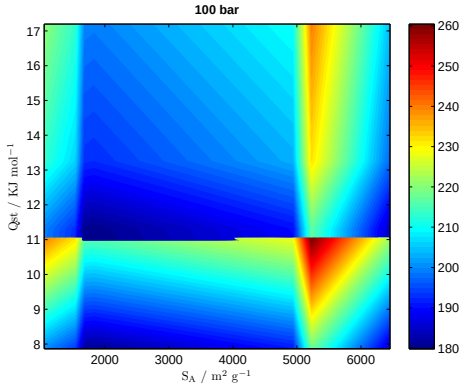

(f) 100 bar

Figure S19: Qst *vs* S_A

Uptake *vs* Qst *vs* Vp

In Figure S11(e), we analized the dependence: uptake *vs* Qst *vs* Vp. Then if we take every surface and make a contour plot we obtain Figure S21 which shows that there are three maxima at the pressure 30 bar, that in absolute uptake units corresponds to:

Qst / KJ mol^{-1}	Vp / cm^3 g^{-1}
10.7	0.55
17.0	0.55
17.0	2.06

However, in delivery amount units, there are four maxima at 30 bar which are (graph is not shown):

Qst / KJ mol^{-1}	Vp / cm^3 g^{-1}
10.7	0.55
17.0	0.55
17.0	2.06
11.0	2.06

Furthermore, in the case of methane uptake in COFs, it seems that Qst is inversely proportional to Vp (Figure S20), however, the two steps relation separating 2D-COFs from 3D-COFs is no longer observed as in the case of Qst *vs* S_A. Once again there is not a theoretical reason for the dotted line to exist, except that to help the eye.

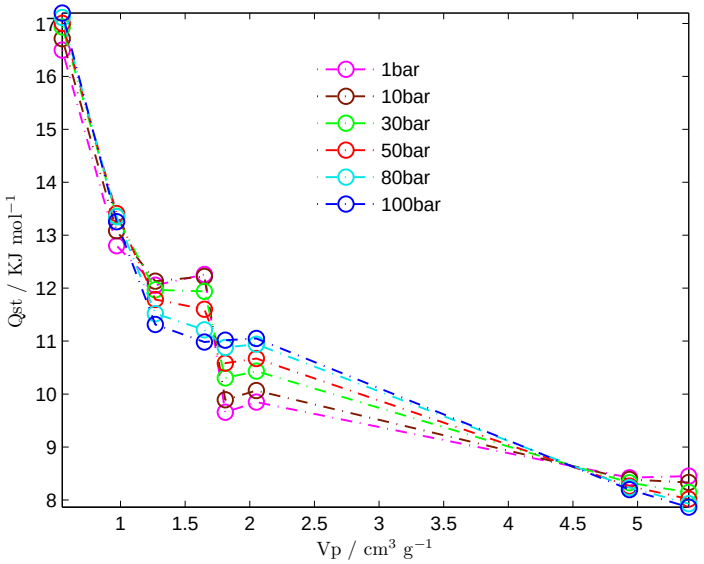

Figure S20: Qst *vs* Vp

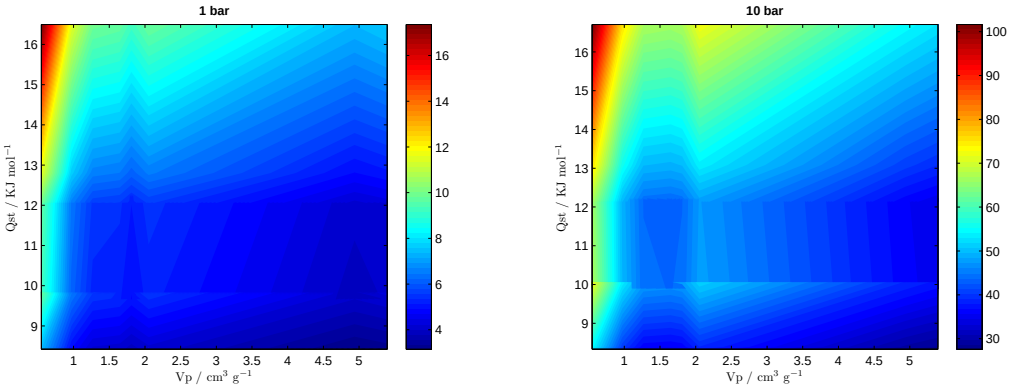

(a) 1 bar

(b) 10 bar

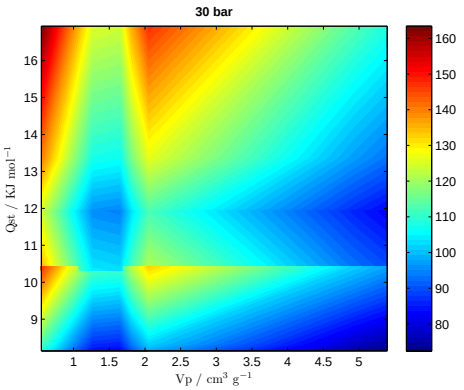

(c) 30 bar

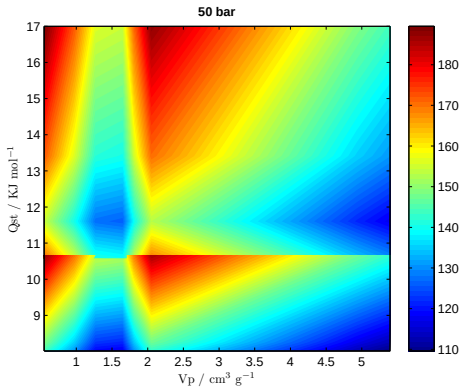

(d) 50 bar

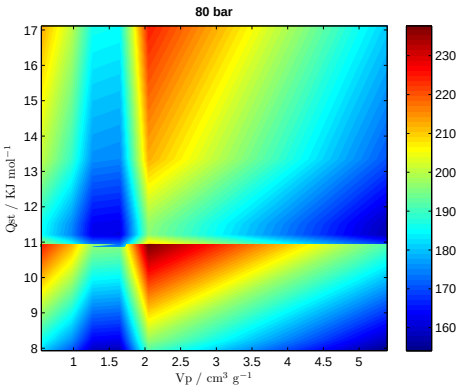

(e) 80 bar

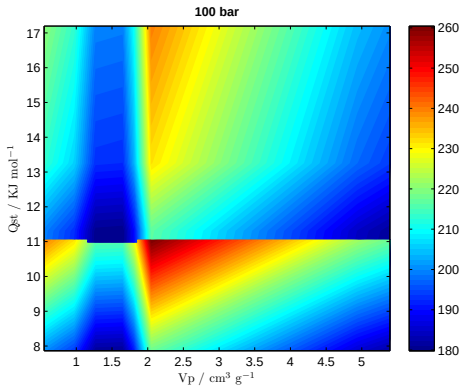

(f) 100 bar

Figure S21: Qst *vs* Vp

Uptake *vs* S_A *vs* Vp

In Figure S11(f), we analized the dependence: uptake *vs* S_A *vs* Vp. Then if we take every surface and make a contour plot we obtain Figure S23 which shows that there are three maxima at the pressure 30 bar, that in absolute uptake units corresponds to:

S_A / m^2 g^{-1}	Vp / cm^3 g^{-1}
1050	0.55
1050	2.05
5230	0.55

However, in delivery amount units, there are four maxima at 30 bar which are (graph is not shown):

S_A / m^2 g^{-1}	Vp / cm^3 g^{-1}
1050	0.55
1050	2.05
5220	0.55
5220	2.05

As it is expected, the S_A is proportional to Vp (Figure S22). In addition, the two steps separating 2D-COFs from 3D-COFs is observed (2D-COFs are located on the left part of the graph while on the right part we find the 3D-COFs).

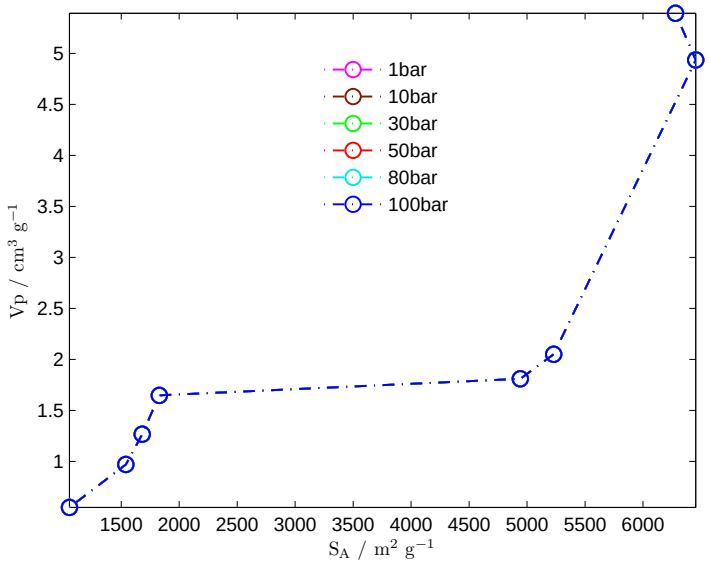

Figure S22: Vp *vs* S_A

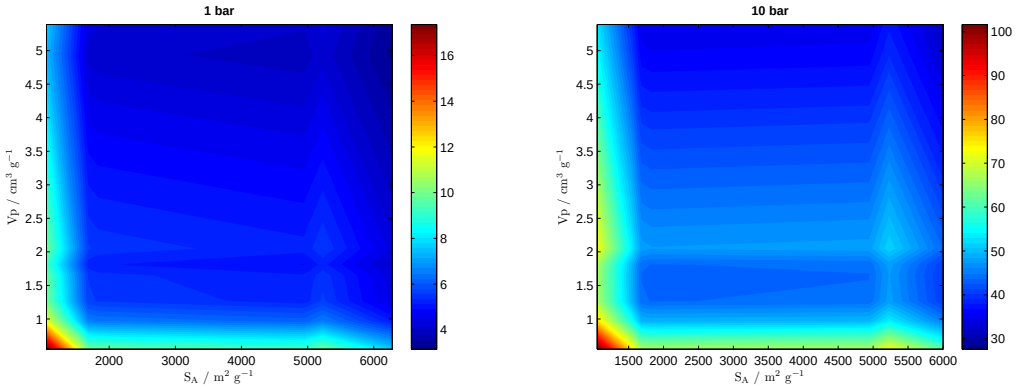

(a) 1 bar

(b) 10 bar

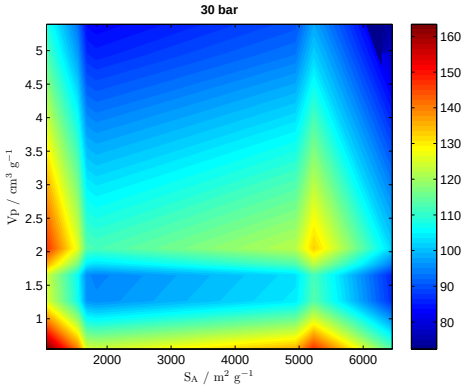

(c) 30 bar

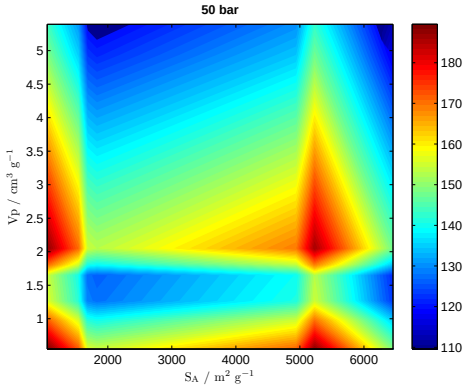

(d) 50 bar

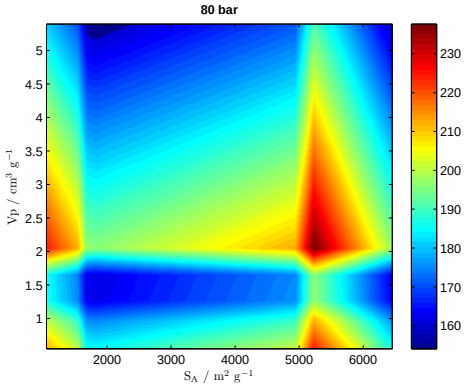

(e) 80 bar

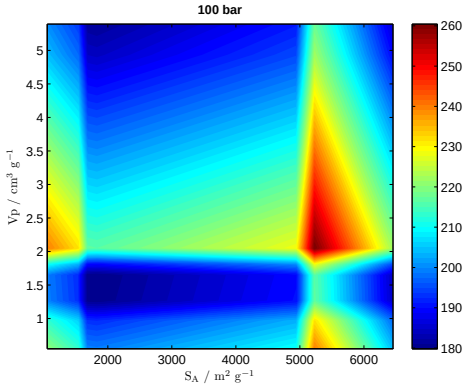

(f) 100 bar

Figure S23: Vp *vs* S_A

Bibliography

[1] (a) Morgan, A. B.; Jurs, J. L.; Tour, J. M. *J. Appl. Polym. Sci.* **2000**, *76*, 1257. (b) Goldschmid, H. R.; Musgrave, O. C. *J. Chem. Soc. C* **1970**, 488.

[2] (a)Côté, A. P.; Benin, A. I.; Ockwig, N. W.; O'Keeffe, M.; Matzger, A. J.; Yaghi, O. M. *Science* **2005**, *310*, 1166. (b)Côté, A. P.; El-Kaderi, H. M.; Furukawa, H.; Hunt J. R.; Yaghi, O. M. *J. Am. Chem. Soc.* **2007**, *129*, 12914.

[3] (a)Lowell, S.; Shields, J. E.; Thomas, M. A.; Thommes, M. *Characterization of Porous Solids and Powders: Surface Area, Pore Size and Density*, Kluwer Academic Publishers, Dordrecht, **2004**. (b)Keller, J.; Staudt, R. *Gas Adsorption Equilibria: Experimental Methods and Adsorption Isotherms*, Springer Science + Business Media, New York, **2005**

[4] NIST chemistry webbook (thermophysical properties of fluid systems); http://webbook.nist.gov/chemistry/fluid/.

[5] Murata, K.; Kaneko, K.; Kokai, F.; Takahashi, K.; Yudasaka, M.; Iijima, S.; *Chem. Phys. Lett.* **2000**, *331*, 14.

[6] Furukawa, H.; Miller, M. A.; Yaghi, O. M. *J. Mater. Chem.* **2007**, *17*, 3197.

[7] (a) Boys, S. F.; Bernardi, F. *Mol. Phys.* **1970**, *19*, 553; (b) Meunier, A.; Levy, B.; Berthier, G. *Theor. Chim. Acta* **1973**, *29*, 49; (c) Jansen, H. B.; Ross, P. *Chem. Phys. Lett.* **1969**, *3*, 40.

[8] Simon, S.; Duran, M.; Dannenberg, J. J. *J. Chem. Phys.* **1996**, *105*, 11024.

[9] Morse, P. M. *Phys. Rev.* **1929**, *34*, 57.

[10] Hättig, C. *Phys. Chem. Chem. Phys.* **2005**, *7*, 59.

[11] Ahlrichs, R.; Bär, M.; Häser, M.; Horn, H.; Kölmel, C. *Chem. Phys. Lett.* **1989** *162*, 165.

[12] Weigend, F.; Häser, M. *Theor. Chem. Acc.* **1997** *97*, 331.

[13] Weigend, F.; Häser, M.; Patzelt, H.; Ahlrichs, R. *Chem. Phys. Letters* **1998** *294*, 143.

[14] Adams, D. J. *Mol. Phys.* **1974** *28*, 5.

[15] Soto, J. L. "Statistical Thermodynamics of Sorption in Molecular Sieves". *PhD Thesis, University of Pennsylvania*, (1979).

[16] National Institute of Standards and Technology "Thermophysical Properties of Fluid Systems" NIST Standard Reference Database, (2005).

[17] Han, S. S.; Deng, W. Q.; Goddard, W. A. *Angew. Chem.-Int. Edit.* **2007**, *46*, 6289-6292.